Engineering Structures 325 (2025) 119487

Contents lists available at ScienceDirect

Engineering Structures

journal homepage: www.elsevier.com/locate/engstruct

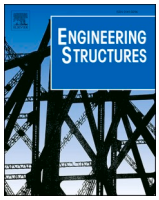

Metamodel-assisted design optimization of robust-to-progressive-collapse RC frame buildings considering the impact of floor slabs, infill walls, and SSI implementation

Iván Negrin [a,*], Moacir Kripka [b], Víctor Yepes [a]

[a] Institute of Concrete Science and Technology (ICITECH), Universitat Politècnica de València, Valencia 46022, Spain
[b] Civil Engineering Graduate Program, Federal University of Technology-Paraná, Via do Conhecimento, Km 1, Pato Branco, Paraná 85503–390, Brazil

ARTICLE INFO

Keywords:
Structural optimization
Progressive collapse
Reinforced concrete
Frame building
Floor slabs
Infill walls
Soil-structure interaction

ABSTRACT

Although mathematical optimization can be a handy tool for structural design, neglecting to consider criteria such as safety can result in designs vulnerable to specific scenarios. One aspect of structural safety that has been gaining interest is buildings' progressive collapse (PC) resistance. Many experimental and numerical studies have been developed on this subject, although few investigations have related it to structural optimization. This paper presents a procedure called Optimization-based Robust Design to Progressive Collapse (ObRDPC) that integrates both topics. This framework incorporates typically overlooked factors, such as including floor slabs and infill walls as part of the superstructure or accounting for soil-structure interaction. The methodology is applied to five case studies of three-dimensional reinforced concrete frame building structures. The results demonstrate the significant influence of slabs and walls on the PC resistance of buildings. Beams are the elements that benefit the most from the presence of both to bridge over the failure of a load-bearing element. On the other hand, increasing the structure levels improves its robustness, contrasting with increasing the span length. The impact of PC-resistant design on beams, columns, and foundations is also evaluated compared to the traditional approach.

1. Introduction

Mathematical optimization is a very useful tool for solving complex structural design problems. However, depending on the optimization problem formulation, this tool can be more or less effective. For example, optimizing economic or environmental aspects may worsen other essential criteria, such as structural safety. Therefore, a wise choice of optimization criteria is essential to make good use of this great tool.

The construction industry is one of the most polluting and resource-consuming sectors [1,2]. Reinforced concrete (RC) frame buildings are an important component of this industry. Thus, their economic and environmental impact is significant. That is why many authors have developed methodologies to apply economic optimization to this type of construction [3,4]. Others have focused on optimizing environmental criteria such as embodied carbon [5,6]. Some studies have compared the results of optimizing both criteria [7]. Other authors have developed multi-objective optimization methodologies, combining criteria such as construction cost with constructability [8], economy with environmental impact [9], the latter with durability and constructability [10], or time, cost, quality, and CO_2 emissions [11]. However, in addition to the criteria mentioned above, aspects associated with the structural safety of buildings have yet to be implemented. The lack of studies that formulate structural safety as part of the design optimization problem of realistic RC buildings may originate in the difficulty of modeling, analyzing, and designing this type of structure. Another cause may be the difficulty of measuring how safe a building is.

One of the phenomena that has been receiving much attention about building safety is the resistance to progressive collapse (PC). Extreme events, such as hurricanes, earthquakes, explosions, vehicle crashes, human error, or terrorist acts, can affect buildings. These events often cause local damage to the building structure, which can trigger a total collapse. Any PC of buildings results in significant losses in both human life and material assets [12,13]. As a result, the U.S. General Services Administration (GSA) [14] and the Department of Defense (DoD) [15] have issued guidelines to reduce the potential for PC in building design. One of the approaches proposed in these guidelines is the Alternate Path (AP) method. It ensures that the structure can withstand the failure of a structural element and localize the resulting damage. The main

* Corresponding author.
E-mail address: ianegdia@doctor.upv.es (I. Negrin).

https://doi.org/10.1016/j.engstruct.2024.119487
Received 6 August 2024; Received in revised form 22 November 2024; Accepted 9 December 2024
Available online 12 December 2024

Nomenclature

AP	Alternate Path.
APM CC	Alternate Path Method removing a corner column.
APM EC	Alternate Path Method removing an exterior column.
B	Beams.
BBO	Biogeography-based Optimization.
C	Columns.
c	Soil cohesion.
CDLIS	Constrained Deterministic Local Iterative Search.
CDLIS 1	Solution found when applying the CDLIS local search algorithm for the first time.
CDLIS 2	Solution found when applying the CDLIS local search algorithm for the second time, also considered as the global optimal.
CP	Coefficient of penalization.
d	Strut diagonal length.
D	Dead load.
DCR	Demand Capacity Ratio.
DoE	Design of Experiment.
e_i	Unit CO_2 emissions.
E	Modulus of elasticity of the soil.
E_c	Concrete elastic modulus of columns.
E_w	Secant modulus of elasticity of masonry infill walls.
F	Foundations.
Fx	Dimension of a foundation base in the x-axis direction.
Fy	Dimension of a foundation base in the y-axis direction.
f_k	Characteristic compressive strength of the masonry.
g_i	Behavioral constraints.
GSA	General Service Administration.
H	Columns height.
H'	Columns free height.
HFS	High-Fidelity Simulation.
I_c	Columns moment of inertia in the longitudinal direction of the wall.
KBO 1	Solution found when optimizing the first Kriging-type metamodel.
KBO 2	Solution found when optimizing the new local Kriging-type metamodel.
k	Soil stiffness coefficient.
K_E	Coefficient used to calculate E_w.
L	Span of each bay of the building.
L_B	Length of the building span on the y-axis.
Li	Live load.
LFS	Low-Fidelity Simulation.
L_L	Length of the building span on the x-axis.
LSP	Linear Static Procedure.
m_i	Measures related to the material/constructive activities units.
N	Number of building levels.
N_B	Number of spans in the y-axis direction.
N_i	Height of each level of the building.
N_L	Number of spans in the x-axis direction.
ObRDPC	Optimization-based Robust Design to Progressive Collapse.
p	Pressure acting on the foundation base.
PC	Progressive Collapse.
$q^*_{br\_II}$	Foundation base bearing capacity pressure.
Q_{AF}	Forces acting on the elements.
Q_{UC}	Unfactored ultimate capacity of the elements.
R'^*	Linearity limit stress of the soil.
RC	Reinforced Concrete.
RDPC	Robust Design to Progressive Collapse.
S	Foundation base settlement.
$\overline{S}$	Foundation base settlement for an acting pressure equal to the base linearity limit stress of the soil.
SSI	Soil-Structure Interaction.
T	Total emissions.
t_w	Thickness of the masonry infill wall.
V_I	Volumetric index.
w	Equivalent strut width.
W	Wind load.
$x1, x2, \ldots, xn$	Design variables.
$tan\ (\alpha)$	Secant stiffness coefficient of the soil during the loading process.
$tan\ (\beta)$	Secant stiffness coefficient of the soil during the unloading process.
γ	Soil density.
ϕ	Soil friction angle.
μ	Soil Poisson's ratio.
θ	Angle formed by the equivalent strut.
λ, λ_h	Parameters used to calculate the equivalent strut width.

objective is to redistribute the gravity loads after removing a load-bearing element [16]. Given the unpredictability of accidental events, this hazard-independent design method is considered one of the most reliable methods for assessing the resistance of building structures to PC [17].

In recent years, many studies have focused on this phenomenon's experimental and numerical study. A common practice in experimental studies is the use of substructures to study the loss of a load-bearing element in typologies such as beam-column frames [18], RC flat plates [19], or precast RC frame structures [20]. Regarding the numerical approach, several studies have comprehensively evaluated the PC of 3D RC buildings against the loss of corner, exterior, and interior columns [21]. Others have also analyzed the consequences of the loss of shear walls located in critical zones of the building [22], or the simultaneous and sequential loss of load-bearing elements [23]. The influence of building height has also been evaluated in detail [24].

On the other hand, one of the important aspects of this topic is the influence of alternative structural elements, such as floor slabs and infill walls, on the PC resistance of buildings. Several experimental studies have demonstrated slabs' influence on the resistance capacity of substructures [25,26] and even of a full-scale building [27]. Regarding structural walls, practical [28] and numerical [29] experiments have proved their influence on building structural robustness. This type of element improves not only the initial stiffness of the structural assembly but also the additional load path produced by its presence, which can mitigate concrete damage at the ends of the beams, thus improving their ductility and reparability. In a study of a full-scale building, [30] analyzed the structural influence of infill masonry walls on aspects such as load redistribution and their alternate paths in the event of the loss of a corner column. This study provides practical recommendations for modeling this type of infill wall, many of which have been adopted in the current research.

However, following the guidelines established by these studies and the corresponding codes to implement robust design to progressive collapse (RDPC), it is straightforward to overdesign the structure. It is here that combining this approach with structural optimization must be crucial in designing safe yet sustainable buildings. Thus, one area that still needs to be solved in this branch is the implementation of studies combining RDPC and structural optimization, even though some authors have proposed some methodologies that integrate both topics. For

example, the design optimization of redundant systems [31], or risk-based design applied to cost-benefit analysis [32,33] and to the optimal design of RC structures [34,35]. Other authors have adopted a deterministic approach combining machine learning as a decision-making technique with a classical heuristic to optimize the design of RC frame buildings [36]. Nonetheless, these studies are limited by simplifications made to the case studies. They consist of substructures or plane frames, and do not consider slabs and walls part of the building frame.

Another common simplification is the non-consideration of the foundations within the structure to be optimized. It causes the supports to be idealized, even though it has been proven that the soil-structure interaction (SSI) is an aspect that significantly influences the behavior of the superstructure in RC frame buildings [37]. In practice, buildings settle, and due to differences in acting loads and foundation shape, these settlements are not equal at all points. It causes additional stresses to be introduced in the superstructure, which changes the structural behavior concerning models with idealized supports. It not only conditions the structural design of the building, but also changes the stress-strain state of the structural elements. Hence, the evaluation of the PC resistance of the structure may be erroneous [38,39].

Therefore, this study aims to overcome all these limitations by integrating RDPC with structural design optimization. The case studies consist of five 3D RC buildings, including the design optimization of the foundations as part of the structural assembly and their interaction with the soil (SSI). Slabs and walls are modeled as part of the superstructure. It allows for evaluating these elements' influence on the building's structural behavior in case of loss of load-bearing elements, as well as the environmental benefit of their presence in designing buildings that are structurally robust to abnormal events. The design problem is formulated as a mathematical optimization problem, where the objective function (CO_2 emissions) serves as a control element while ensuring structurally robust design in the form of constraints. In other words, safety and structural robustness are guaranteed while minimizing the environmental impact of the building construction. This environmental criterion is chosen because by optimizing this indicator, other economic and environmental indexes are also significantly improved. Considering all these aspects makes solving the optimization problem very complex, especially from the computational point of view. Consequently, a metaheuristic consisting of a biphasic search based on Kriging-type metamodels is designed, including local optimization procedures to refine the search for the best solutions.

2. Methodology

The methodology begins with a description of the case studies. The Alternate Path method is also introduced, as well as how floor slabs and infill walls are modeled. Subsequently, the proposed general methodology, i.e., the Optimization-based Robust Design to Progressive Collapse (ObRDPC) framework, is described. Here, the objective function, variables, and constraints of the resulting optimization problem are established. Then, it is explained how the SSI is modeled within the ObRDPC framework. Finally, the strategy for solving the formulated complex optimization problem is presented.

2.1. Problem description

This research is based on five reinforced concrete frame buildings as case studies. The primary case has three bays in both directions, with four levels. Each bay has a length L of 4 m. The other cases start from this one, increasing the number of levels (N) to five (case 2) and six (case 3) keeping $L = 4$ m, and the length of the bays to 6 (case 4) and 8 m (case 5) keeping $N = 4$. In all cases, the story height (N_i) is 3.5 m. Fig. 1 represents the five case studies.

The superstructure model is based on frame-type elements (beams and columns). This study also includes slabs and walls as elements that contribute structurally to the building frame. The floor slabs are structurally connected to the beams, while the walls are considered to be masonry and, therefore, have a structural nature. The modeling of these elements is detailed below. The cross sections of the frame elements are rectangular. An aspect of notable relevance is the modeling and design optimization of the foundations as part of the structural assembly, as well as their interaction with the soil. In this case, the shallow single-footing variant has been selected because of its good adaptation to the type of building investigated. The foundation footings are modeled as shell elements. They are discretized (meshed) to improve their behavior

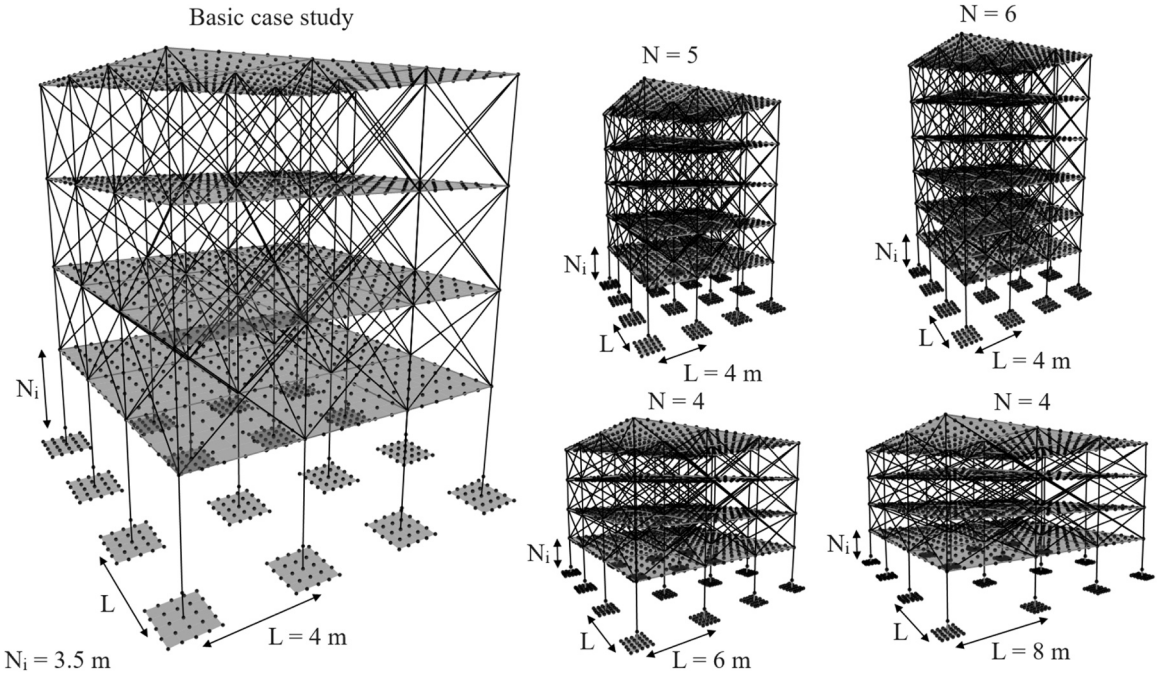

Fig. 1. Five case studies considering the modeling of foundations, floor slabs, and infill walls. The latter are modeled as strut-type elements, as discussed in Section 2.1.2.

as slab footings. A sensitivity analysis concludes that four divisions in each direction are sufficient to obtain accurate structural behavior results (see Section 2.3).

Another important aspect is the realistic design of the elements. Beams, columns, and foundations are automatically designed with the actual steel area. That is, from the steel area required by calculation, a realistic distribution of the reinforcing bars within the concrete sections is made. For the case of frame-type elements (beams and columns), this area is obtained from the structural software SAP2000 and converted into a real solution to get the planar layout of reinforcement within the cross-section. Each solution is checked for compliance with the constraints explained later. In addition, reinforcing bar cutoff and detailing are performed, as shown in Fig. 2. It is done using a tool programmed in Matlab. In the case of foundations, the programmed tool performs the geotechnical and structural design. The possibility of communicating the SAP2000 software with programming languages such as Matlab through CSi API functions makes it possible to fully automate the process and assemble it to the optimization procedure. For more information on these procedures, consult [40].

The traditional approach uses the Limit State method based on the ACI 318–14 code. The most essential load combinations are shown in Eqs. 1–4. Here, *D*, *Li*, and *W* are the dead, live, and extreme wind loads, respectively. It should be highlighted that other load combinations are used to design the foundations and check the serviceability limit state. The applied load values are shown in Table 1.

$$1.2D + 1.6Li \tag{1}$$

$$1.2D + 0.8W \tag{2}$$

$$1.2D + 1.4W + 0.5Li \tag{3}$$

$$0.9D + 1.4W \tag{4}$$

2.1.1. Alternate Path method

One of the alternatives proposed by codes such as GSA to apply the RDPC is the Alternate Path method. As the overall approach is static, the analysis will be implemented using the Linear Static Procedure (LSP). According to [29], this approach can be used to evaluate the PC potential of existing or proposed structures. Furthermore, according to GSA guidelines, the buildings used in this study are suitable for analysis using this method. All structural elements are considered primary, i.e., they provide capacity to the structure to resist the collapse due to removing a vertical load-bearing element. The load combination shown in Eq. 5 is applied on the spans adjacent (at all levels) to the removed column (see Fig. 3). The same combination is applied in the rest of the superstructure but without the dynamic amplification factor equal to 2.0.

$$2.0[1.2D + 0.5Li] \tag{5}$$

The methodology proposed in this study makes some simplifications regarding the original method. These simplifications are due to the need

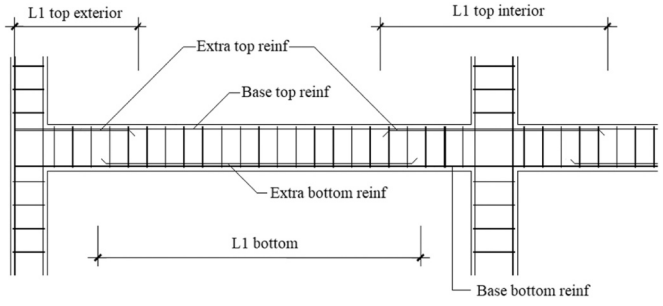

Fig. 2. Configuration of reinforcing steel in frame elements, with actual distribution and cutoff/detailing of steel bars.

Table 1
Loads considered.

Description	Value	
Dead load on lower floors	4.80 kN/m^2	
Dead load on roof	5.40 kN/m^2	
Live load on lower floors (Offices)	3.00 kN/m^2	
Live load on roof	0.80 kN/m^2	
Wind load	Positive pressure	Negative pressure
	0.92 kN/m^2 0 −5 m,	0.50 kN/m^2 0 −5 m,
	1.01 kN/m^2 at 7 m,	0.55 kN/m^2 at 7 m,
	1.13 kN/m^2 at	0.62 kN/m^2 at
	10.5 m,	10.5 m,
	1.25 kN/m^2 at 14 m,	0.69 kN/m^2 at 14 m,
	1.37 kN/m^2 at	0.76 kN/m^2 at
	17.5 m,	17.5 m,
	1.50 kN/m^2 at 21 m.	0.83 kN/m^2 at 21 m.

to convert the cumbersome iterative checking procedure proposed by codes such as GSA into an automated design process. Therefore, instead of implementing a trial-and-error method, the structure is designed to directly meet the criteria established in these codes. As a result, this methodology that enables structural robustness can be inserted into the building design optimization problem. It is important to note that the proposed framework encompasses several factors that make a single design procedure extremely complex. If we add that structural optimization requires repetition of these design procedures, the whole problem becomes even more complicated to solve. Therefore, these simplifications adopted when implementing the AP method are essential to improve the computational efficiency of the procedure considerably.

These simplifications are based primarily on the unification of both action components (force- and deformation-controlled actions) in the same procedure. The codes establish differences in the processes for evaluating each component, which makes the approach laborious to execute. In this study, the first simplification is to use the same load amplification factor of 2.0 for both action components, as shown in Eq. 5 [29,41,42].

On the other hand, one of the fundamental aspects of the AP method is the acceptance criteria. For the LSP, the PC potential of a structure is evaluated by checking each structural member's demand capacity ratio (DCR), as shown in Eq. 6 [29]. Here, another simplification is introduced. It is implemented that for both action components, the DCR values must be less than 1.0. In codes such as GSA, this DCR limit for deformation-controlled actions must be calculated using an extremely laborious procedure. In the case of force-controlled actions, the acceptance criterion in the codes establishes that the DCR must be less than 1.0. It is also another simplification on the safety side since some authors establish that DCR values can reach 1.5 and avoid the collapse of the structure. That is, some damage to the element is allowed [29]. Thus, this simplification may be conservative, but in addition to increasing the structural safety of the building, it ensures that the intervention after the extreme event is minimal [43]. In Eq. 6, Q_{AF} represents the forces acting on the elements, which can be bending, axial, or shear forces. Q_{UC} represents the unfactored ultimate capacity of the elements, which can also be bending, axial, or shear resistance.

$$DCR = \frac{Q_{AF}}{Q_{UC}} \tag{6}$$

As can be seen, the implemented simplifications mainly focus on deformation-controlled actions. Therefore, another acceptance criterion is introduced to increase control in this field. It consists of limiting the rotation angle of the beams to 4°, as [41] suggested for the case of doubly reinforced concrete beams when the tension membrane is not included in the analysis. For this study, the analysis does not consider the action of the tensile membrane, mainly due to the lack of control over the slab design. Therefore, the reinforcement steel characteristics of both the slabs and the connection with the beams are ignored, although it is

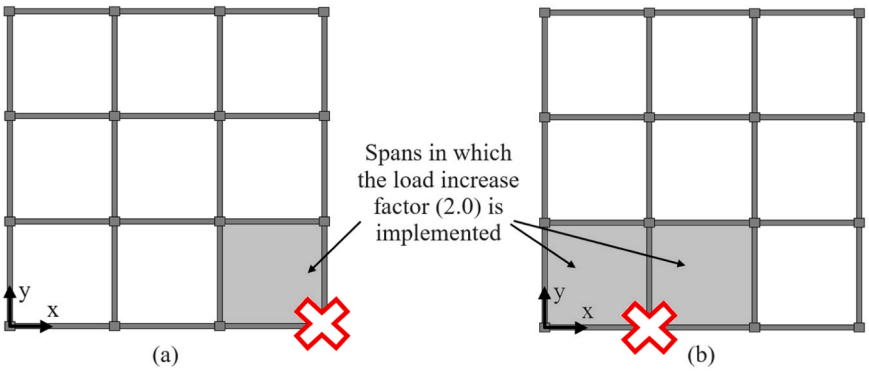

Fig. 3. First level exterior column removal scenarios: (a) corner column, (b) exterior column.

assumed that there is continuity in the direction perpendicular to the beams (vertical displacements). On the other hand, this connection is represented in the model as discrete points, as shown in Fig. 4a. This lack of continuity means that the tensile membrane action of the slab on the beam is not adequately represented. Therefore, given all this uncertainty, it is considered that there is no tensile membrane action, and the critical acceptance criterion is assumed. Note that, when considering this phenomenon, the limit of the beam rotation angle increases to 12° [41]. With all this uncertainty, the best alternative is the most critical option. Thus, limiting the rotation angle of the beams to only 4° guarantees the non-occurrence of excessive deformations so that, as assumed, the tensile membrane action of the slab does not occur. In addition, this acceptance criterion with the most critical condition ensures greater control of deformations, which is what was sought in principle.

All these simplifications make it possible for the structural software to design the structure based on the design forces obtained in the damaged model with their corresponding load combinations. Instead of proposing designs and checking whether they meet the acceptance criteria iteratively, our methodology proposes a design that already meets these criteria. Therefore, it is moved from a manual trial-and-error procedure to an automated design optimization one, as summarized in Section 2.2.

Another key point of the AP method is the position of the elements to be eliminated. According to [44], corner columns are possibly one of the most exposed and vulnerable structural components of a building. Protecting exterior columns from blast or impact is usually more challenging than interior columns. Considering this statement and following the recommendations set out in GSA for removing these load-bearing elements, two failure scenarios are established. The first is removing a corner column (Fig. 3a). The second is removing an exterior one (Fig. 3b). It is important to note that, due to the configuration of the variables, the design is symmetrical. Therefore, when considering the failure of one element and extending the design to analogous zones, the other elements are designed to resist the failure in their zone. In other words, the structure's final design is configured to cope with the failure of any element analogous to the one assumed to fail.

2.1.2. *Modeling of floor slabs and infill walls*

As mentioned, the slabs are considered solid, 12 cm thick, and are

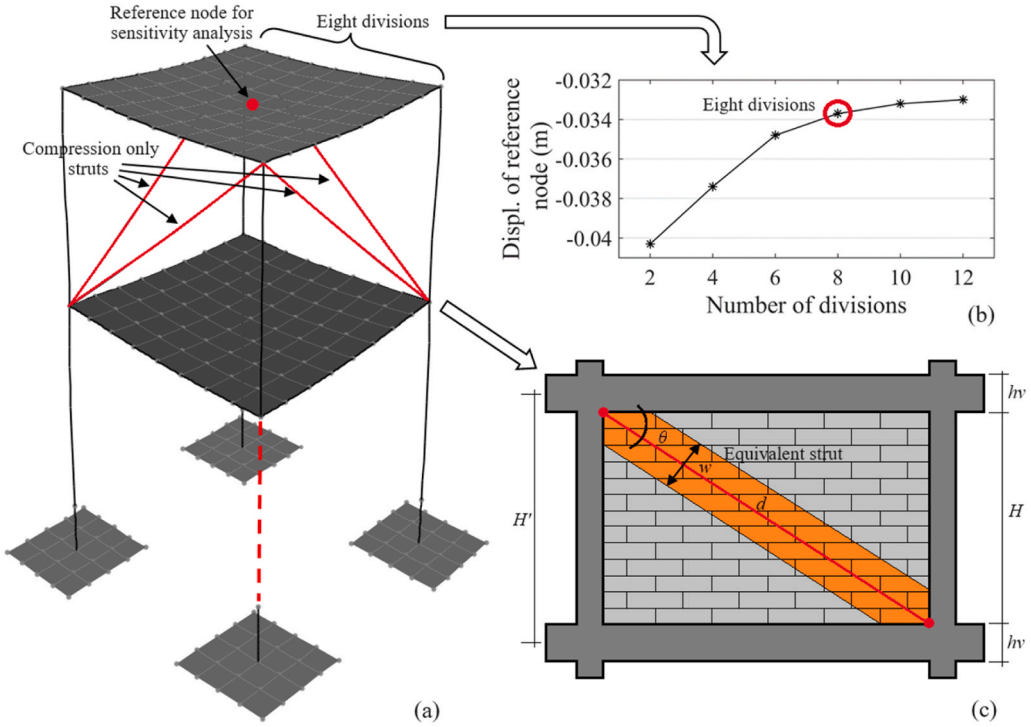

Fig. 4. (a) Modeling of slabs and walls as part of the RC frame structure, (b) sensitivity analysis to determine the ideal number of divisions for shell-type elements simulating slabs, and (c) geometric parameters defining the properties of the equivalent strut that simulates the infill walls.

modeled as shell elements. These are discretized to make their structural behavior more realistic, especially their interaction with the beams. It is assumed that the slab-beam connection is made in such a way that there is continuity in the vertical direction. Therefore, both elements deform together. Discretization is fundamental to achieving this effect. Thus, the more the slab is divided, the more realistic the behavior is. However, it also makes the model "heavier". A sensitivity analysis is performed to find a balance, as shown in Fig. 4b. For this case, the deformation at the center point of the slab is measured for the same load combination as a function of the number of splits. In the figure, it can be seen how, from eight divisions onwards, the behavior stabilizes. Then, each slab is divided into eight parts in each direction.

On the other hand, the modeling of infill walls is a more complex phenomenon. Thus, instead of modeling this element as is done for slabs, an alternative procedure is used. The masonry assembly is replaced by a single equivalent elastic diagonal strut, acting only in compression (Fig. 4a and c). This methodology has been validated in a full-scale experimental study [30].

As mentioned, the infill walls are considered masonry, and the mechanical properties of both mortar and bricks are taken from the experimental study by [30]. The secant modulus of elasticity E_w is calculated using Eq. 7.

$$E_w = K_E \bullet f_k \tag{7}$$

Here, the coefficient K_E is taken as 550 as per ASCE/SEI [45]. In the study [30], it was demonstrated that this is the value that most closely matched the real experiment. On the other hand, f_k is the characteristic compressive strength of the masonry. It is equal to 6.97 MPa, as obtained in this practical experiment. Therefore, $E_w = 3834$ MPa. From here, the equivalent strut width w is calculated according to Eqs. 8, 9 and 10, as is done in codes such as ASCE/SEI 2007.

$$w = 0.175\lambda_h^{-0.4} d \tag{8}$$

$$\lambda_h = \lambda H' \tag{9}$$

$$\lambda = \sqrt[4]{\frac{E_w t_w \sin 2\theta}{4E_c I_c H}} \tag{10}$$

Here, d is the diagonal length, H' is the free height, t_w is the thickness of the masonry infill wall (113 mm in this case), θ is the angle formed by the equivalent strut, E_c is the concrete elastic modulus of columns, I_c is the columns moment of inertia in the longitudinal direction of the wall, and H is the columns height. These parameters are shown in Fig. 4c.

As shown in Fig. 4a, the struts are only located at the upper levels. It is considered that no structural walls are placed at the lower level since these locals are assumed to be intended for stores (with glass walls or similar). Another aspect to highlight is that in Fig. 4a, only the struts working in compression are shown. In Fig. 1, where the case studies are represented, two struts per span can be seen. In the structural model, the "compression-only" function is assigned to each strut-type element, so only the one that works in compression will be activated.

2.2. The ObRDPC framework

Everything explained above about the traditional design and AP method is summarized in the flowchart in Fig. 5a. In general terms, the optimization method "drives" the process by assigning values to the design variables. Subsequently, the structural software SAP2000 is automated to model the structure according to the design variables. The analysis is then run, and data is stored, for example, to design the foundations (support reactions). These data are also used to check constraints, such as the horizontal displacement of the structure. Once the analysis is run, the software designs the frame-type elements, as established in previous sections. It has already been mentioned that, in this case, the program provides the reinforcement area required for the concrete sections proposed by the optimization algorithm. Once all this information is stored, the SAP2000 is closed, and the programmed tool proceeds to the final design of all the elements and the checking of the constraints. Finally, the emissions required to construct the proposed building are calculated, and the optimization algorithm analyzes this value to reassign values to the variables and repeat the procedure. Each of these processes is called function count, i.e., a procedure in which the optimization algorithm assigns values to variables and obtains an answer from the objective function.

Within each function count there are two design procedures. The first one refers to the classic design, which is similar to previous research [10, 37]. As for the RDPC (second design procedure), the AP method is implemented, converting the manual and iterative checking process into

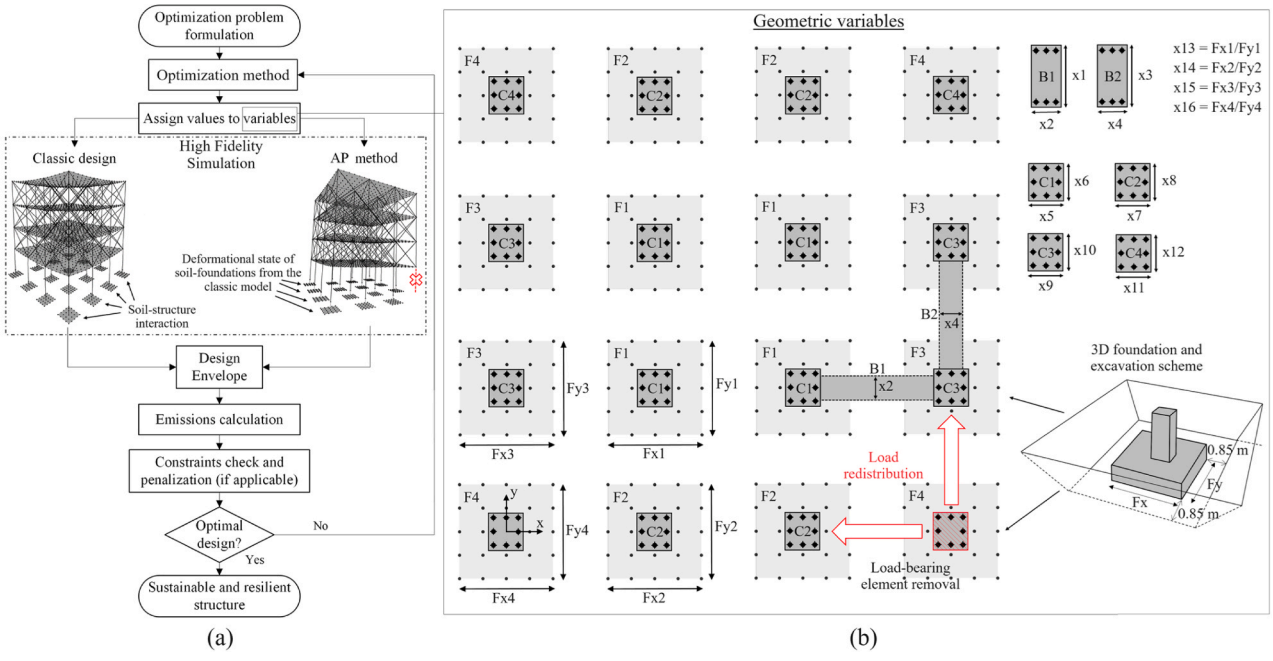

Fig. 5. (a) General flowchart of the ObRDPC (SSI is explained in Section 2.3), (b) plan view of the graphical representation of geometric variables.

an automatic direct design one. The load-bearing element is eliminated, and the load conditions and combinations are established depending on the location of the eliminated element. The influence of the SSI from the classical model is also included in the damaged model (see Section 2.3). Instead of establishing the revision procedure proposed by the related codes, a direct design approach is adopted. The model is assigned the dimensions of the cross-sections proposed by the optimization algorithm in the traditional design. Based on these dimensions and the design forces Q_{AF} of the damaged model (including the SSI effects from the conventional model), the required steel areas are calculated. In this way, the resistant capacity Q_{UC} is automatically higher than Q_{AF}, and the DCRs are less than 1.0 for both force- and deformation-controlled actions. These areas are transformed into real solutions. The foundations are also designed geotechnically and structurally for this failure state (without applying the dynamic amplification factor). These results are stored and compared with those obtained with the classical design to select the critical ones (design envelope). With this global design, the value of the objective function is calculated, and it is checked that this global design meets the structural requirements in the form of constraints. If non-compliance, the objective function is penalized, and the optimization algorithm assigns new values to the variables. This process is automatically repeated until an "optimal" design is obtained according to the formulated objective function. At the same time, the proposed building is robust to PC.

2.2.1. Objective function

The objective function of this design optimization problem is CO_2 emissions, as established in Eq. 11. This environmental indicator has been selected because it has proven to be an excellent alternative for the design optimization of this type of structure. Its use provides outstanding results in other indicators such as monetary cost (economic criterion) or embodied energy (environmental criterion) [7]. Within the ObRDPC framework, the objective function serves as a control element since it is minimized while the structure seeks a configuration that allows it to be robust to PC, in addition to meeting all the other constraints.

$$CO_2 emissions = \sum_{i=1,n} e_i \times m_i(x1, x2, \ldots, xn) \tag{11}$$

Here, e_i represents the unit CO_2 emissions, m_i are the measures relative to the material/constructive activities units as a function of the design variables ($x1$, $x2$,…, xn). The values shown in Table 2 are obtained from the 2016 database of the Institute of Construction Technology of Catalonia [46]. These emission values are related to the use of building materials in the different phases of production and placement. Consequently, the higher this value, the lower its sustainability.

2.2.2. Variables

All variables in these problems are discrete in obtaining practical engineering solutions. The first four variables regulate the dimensions of the cross-sections of the beams and are limited to values multiples of 5 cm. All beams are grouped into two geometry groups: interior and exterior. Therefore, all interior beams will have the same section, while the exterior beams will have a different one. This is done due to the symmetry of the structure and obeys constructive or architectural criteria. Those regulating the element depth ($x1$, $x3$) take eleven possible values, depending on the length of the spans. To set the lower limit, the span L is divided by 18 and adjusted to be a multiple of 5 cm. The upper limit is set so that the variable can take the abovementioned eleven values. For example, for buildings of $L = 4$ m, the depths of the beam sections can vary from 0.25 to 0.75 m. For $L = 6$ m, it would range from 0.35 to 0.85 m, and so on. Those related to the width ($x2$, $x4$) can take five values, starting at 0.20 m for the $L = 4$ and 6 m buildings and increasing that lower limit to 0.25 m for the 8 m span building.

The other eight variables regulate the dimensions of cross-sections of each column geometry group: interior ($x5$, $x6$), exterior on the x-axis ($x7$, $x8$), exterior on the y-axis ($x9$, $x10$), and corner ($x11$, $x12$). The first of the two variables handles the side in the x-axis direction. The second one regulates the side in the y-axis. These variables are also limited to multiples of 5 cm and vary from 0.25 to 0.60 m to take eight possible values. The other four variables control the rectangularity of the base of each foundation group: interior ($x13$), exterior in the x-axis ($x14$), exterior in the y-axis ($x15$), and corner ($x16$). Each foundation group can take nine values of rectangularity, i.e., [0.50, 0.63, 0.75, 0.88, 1.00, 1.25, 1.50, 1.75, 2.00]. Fig. 5b graphically represents each of these variables. Finally, the last three variables are related to the type of concrete (see Table 2) to be used in beams ($x17$), columns ($x18$), and foundations ($x19$). Therefore, the problem is formulated with a total of 19 discrete variables.

Alternatively, another type of grouping exists that does not affect the number of variables. This grouping relates to the design and configuration of reinforcing steel and is known as "design groups." For architectural and construction consistency, many elements share identical dimensions (geometry groups, which govern design variables). However, reinforcement configurations vary depending on the position of the element to which they belong.

Beams, for instance, are divided into two design groups per level: interior and exterior. Each level has its own independent design groups. Thus, a four-level structure comprises eight beam design groups, while a five-level structure has ten, and so forth.

Columns, in contrast, are grouped every two levels, maintaining four column types per level (interior, exterior along the x-axis, exterior along the y-axis, and corner), similar to the geometry grouping. For a four-level structure, eight column design groups are distributed across levels 1–2 and 3–4. Structures with five or six levels add four groups to cover levels 5 or 5–6, respectively.

Significantly, variations in span length do not affect these design groupings. This geometry/design grouping approach ensures homogeneity, enhancing the construction process and enabling the application of RDPC results to equivalent locations where load-bearing element failures are simulated.

Table 2
Unit CO_2 emissions for materials and activities.

Material		Units	CO_2 em (kg)
Formwork		m^2	2.53
Steel (G−60)*		kg	3.01
Concrete 25 MPa		m^3	244.94
Concrete 30 MPa		m^3	279.21
Concrete 35 MPa		m^3	305.96
Concrete 40 MPa		m^3	307.06
Activities			
Concrete placement	Beams	m^3	34.72
	Columns	m^3	37.20
	Found	m^3	19.84
Earthwork	Excavation	m^3	3.99
	Refill	m^3	12.80

* fy = 420 MPa, Es = 220 GPa

2.2.3. Constraints

In this type of problem there are two types of constraints. The first are called design constraints. These directly regulate the limits of variable movements (boundaries) and are formulated for various reasons such as constructive, architectural, and the like. The other group is more complex, called behavioral constraints. They are responsible for ensuring that the elements comply with both the Limit States and the constraints of the AP method. Eq. 12 represents the classical formulation of behavioral constraints.

$$g_j(x1, x2, \ldots, xn) \leq 0 \tag{12}$$

The constraints related to the strength (ultimate) Limit State of the RC elements are automatically satisfied by calculating the steel area required for the cross-sections proposed by the optimization algorithm.

This also applies to the design approach based on the AP method. On the other hand, the constraints related to compliance with the Serviceability Limit State are deflections in beams for the traditional design approach, limit displacement at the top of the building, cracking of the concrete elements, among others. Another group of behavioral constraints includes the constructability of the RC elements (allowable reinforcement bar spacing) or the limitation of the rotation angle of beams in the AP method. The way to check these constraints is that when any of them is not met, the value of the objective function for the current solution is penalized so that the algorithm discards it as feasible. This penalty is directly proportional to the number of constraints violated, i.e., the penalty coefficient increases as the number of violations increases. For a more detailed report on this type of problem formulation, see [10,37].

2.3. SSI modeling within the ObRDPC framework

Soil-structure interaction is generally ignored in the optimization of building design due to the complexity of its modeling, even though its importance in the efficient design of the superstructure has been demonstrated [37]. Regarding its effect on assessing the PC resistance of buildings, some investigations have numerically proved that its influence is significant [38,39].

However, due to the lack of experimental studies on the behavior of the soil-foundation joint during the failure of a bearing element, this research assumes that the deformational state of the soil during the occurrence of this phenomenon remains constant. That is, the supports remain rigid. This is assumed since the extraordinary event is not long enough in time to cause additional deformations in the soil, which is already supposed to be sufficiently compacted.

Conversely, what happens between the foundation and the soil before the loss of the bearing element is relevant. During its regular behavior stage, the foundation settles, which modifies the initial conditions of the structure at failure [37,40]. Therefore, the consideration of the SSI modifies the stress-strain state of the superstructure when the bearing element is lost, which influences the evaluation of the PC resistance of the building. On the contrary, if rigid supports are considered (as is usually done in this type of design optimization problem), the structural elements will have a different design, and the evaluation of the PC resistance will be wrong.

The hypothesis behind this phenomenon is that the superstructure modeled with classical supports will be under-designed. That is, with less material than if the foundations and their interaction with the soil are modeled. It is due to differential settlements between adjacent foundations caused by differences in shape and acting loads, as in practice. These differential settlements, even within a permissible range, introduce additional stresses in the superstructure, mainly caused by increased deflection compared to a rigidly supported structure.

The soil is modeled as a linearly elastic half-space (Fig. 6a). This study assumes a single homogeneous soil stratum with the following properties: $E = 12000$ KPa (modulus of elasticity), $\gamma = 19$ kN/m^3 (density), $c = 60$ KPa (cohesion), $\phi = 8°$ (soil friction angle), and $\mu = 0.40$ (Poisson's ratio). The foundation is considered as a shallow slab footing. The pressure-settlement relationship is used to model the soil stiffness. Several authors have validated this strategy for different soil types [37]. The pressure-settlement curve (p vs. S) proposed by [47] represented in Eq. 13 (Fig. 6b) is used to establish this relationship.

$$S = \frac{p \cdot \overline{S} \cdot \left(\left(\frac{q^*_{br\_II}}{R'^*} \right) - 1 \right)}{q^*_{br\_II} - p} \tag{13}$$

Here, $\overline{S}$ is the base settlement for an acting pressure equal to the base linearity limit stress of the soil R'^*, and $q^*_{br\_II}$ is the base bearing capacity pressure, based on expressions from plasticity theory. Eq. 14 is used to obtain the soil stiffness coefficient k. The angle α is represented in the curve of Fig. 6b.

$$k = \tan\alpha = \frac{p}{S} = \frac{q^*_{br\_II} - p}{\overline{S} \cdot \left[\left(\frac{q^*_{br\_II}}{R'^*} \right) - 1 \right]} \tag{14}$$

This coefficient k is applied to the nodes resulting from the foundation footing meshing according to their tributary area. Each node will have a different coefficient depending on its position (interior, exterior, or corner) and the foundation to which it belongs. All this, added to the fact that each spring corresponding to each node deforms according to its stiffness, but also to the acting loads, makes the foundation base behave realistically (see Fig. 6c). Quite different from the idealized supports usually implemented. For more information on the modeling of the SSI, refer to [37].

The automatic implementation of this phenomenon within the ObRDPC framework has its special considerations. Recall that its influence is only considered at the stage of regular behavior of the structure (phase 1), changing the stress-strain conditions of the building at the beginning of the extreme event. Fig. 7 shows a diagram with each step for considering the SSI. First, it is started with the traditional model using idealized supports (fixed in this case). The analysis is run for the solution being analyzed, the first foundation design is made, and the k coefficients are calculated for each foundation group. In step 2, foundations and coefficients are included in the initial model. The analysis is rerun, this time using a more realistic model. The foundations are redesigned again, and the k coefficients are updated to match the new conditions. In step 3, the new foundations are modeled, and the updated

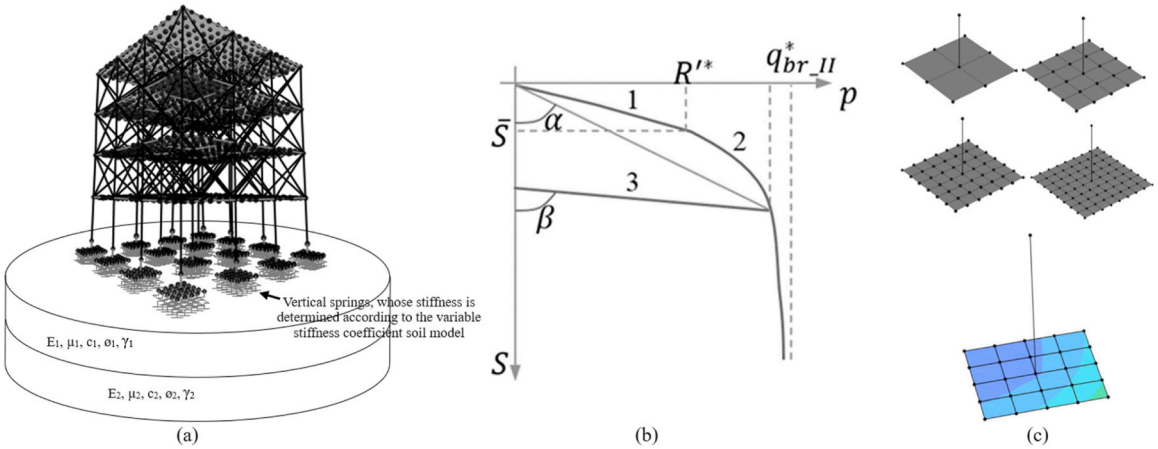

Fig. 6. Concepts related to SSI modeling; (a) General considerations (E, μ, c, ϕ, and γ are soil parameters); (b) pressure-settlement curve (p vs. S); (c) top: meshing of the shell elements of the foundation base, bottom: non-uniform pressure distribution for a foundation case.

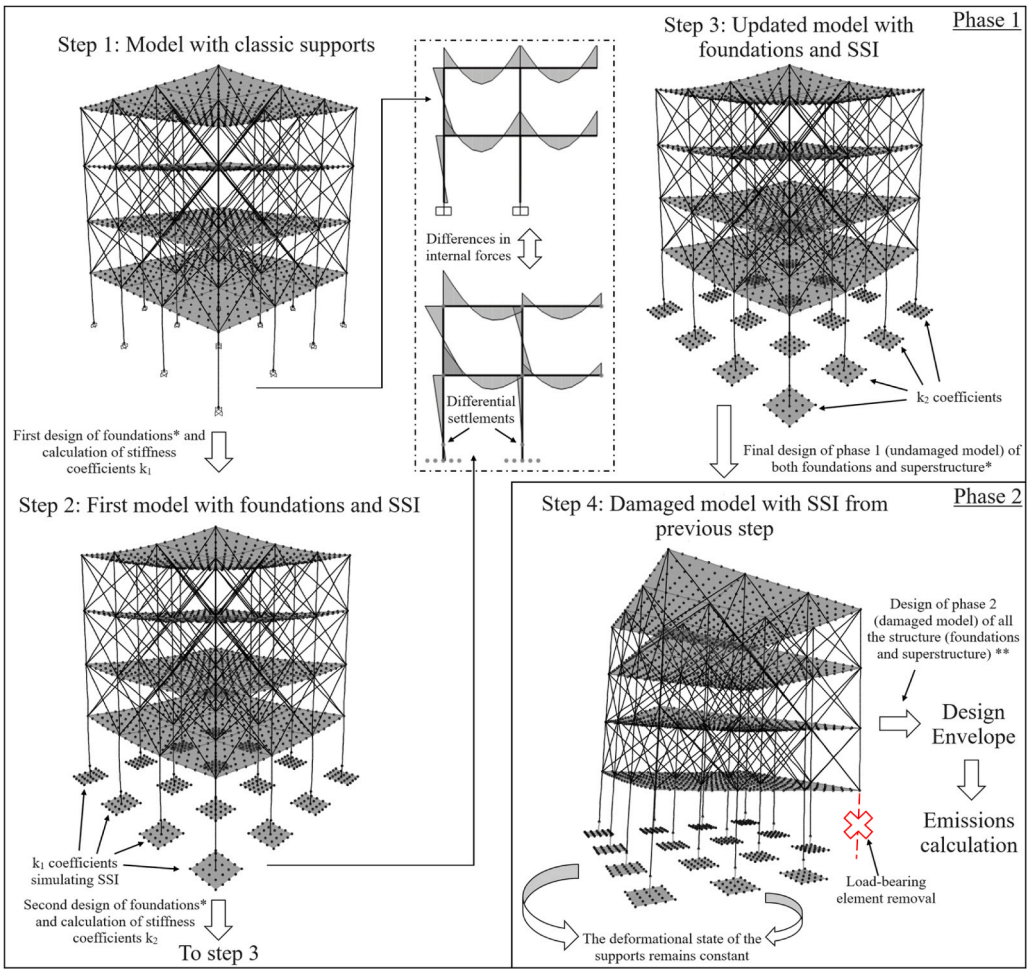

Fig. 7. Implementation of SSI within the ObRDPC framework. * Regular load combinations. * * Load combinations of the AP method according to GSA, the load increase factor is not considered for foundation design.

coefficients are included. The analysis is run again, and the entire structure (superstructure and foundations) is designed this time. All the design results are stored, and this concludes what we call phase 1, or the regular behavior of the structure. The deformational state of the foundations and the top node where the column is to be removed is also stored.

Phase 2 simulates the failure of the load-bearing element. It is eliminated, and the deformational state of the previous phase is included. This deformational state of the foundation remains unchanged, as explained at the beginning of the section. With the AP method's state and load combination, the analysis is run, all elements are designed, and the results are saved. From here, the final part proceeds, as shown in the figure and as described in Section 2.2 (also in Fig. 5a).

2.4. Metamodel-assisted optimization

The above (ObRDPC, SSI, models with slabs and walls) make the optimization problem extremely expensive to solve by traditional methods. The process of modeling, analysis, and structural design using the building model is called, in optimization terms, high-fidelity simulation (HFS). A single HFS is computationally expensive, so the thousands required by conventional heuristics make the procedure almost prohibitive. A very efficient alternative for these cases is metamodel-assisted optimization. I.e., creating a model of the actual model, which is much simpler to evaluate than the complex model, and using it as a surrogate for the real one in the optimization process. These simulations using the metamodel are called low-fidelity simulations (LFS).

An initial population of real values must be created using HFS to build a metamodel, i.e., the so-called Design of Experiment (DoE). From this cloud of points, the metamodel is constructed. There are several techniques for both the DoE and the construction and validation of the metamodel itself. The most commonly used combination in structural design optimization is Latin Hypercube Sampling (LHS) for the DoE and Kriging-type strategies for constructing the metamodel [48]. Hence, in this study, we implement a variant to the one proposed by [37] consisting of a biphasic search combining LHS-Kriging. It is also used a local search algorithm called Constrained Deterministic Local Iterative Search (CDLIS) proposed in the previously referenced study, which is improved for this research. The proposed methodology includes a traditional heuristic called Biogeography-based Optimization (BBO) as a base method, proposed by [49]. This heuristic has shown excellent results for this type of discrete structural optimization due to its particular recombination operator [50].

It is essential to point out that for the construction of the metamodel, the space of solutions is restructured since, in the previous study, it was proved that the Kriging-type metamodels lose effectiveness when the number of variables is large compared to the number of values that they can take. It makes the space of interior solutions minimal compared to the number of solutions at the boundaries. That is why the 19 variables (with an average of 8 possible values) become 5, grouping (1) the beams, (2) the "interior" and "exterior on x-axis" columns, (3) "exterior on y-axis" and "corner" columns, (4) the foundations, and (5) the concrete quality in the different structural elements. The number of variables decreases

considerably and increases the average number of possible values each variable can take to approximately 3568. It makes the interior solution space much larger than the number of variables. BBO parameters are tuned (using LFS) to solve these 5-variable problems as efficiently as possible. However, the CDLIS algorithm is designed for problems like the original one: many variables compared to the values they can take. That is why the problem is returned to its original 19-variable version when performing local optimization. Another aspect of relevance is the establishment of the coefficient of penalization (CP). Through a trial-and-error procedure, and using information from previous studies, it was decided to penalize the solution with a 15% increase (CP = 1.15) when it violates one constraint, 30% when it violates two, 45% when it violates three, and 60% when it violates four or more.

By optimizing one case study with the traditional heuristic (BBO) and checking the efficiency (accuracy and computational savings) of the proposed methodology, the remaining cases are optimized directly with the metaheuristic approach. Three procedures are performed for each case. The proposed strategy is graphically described in Fig. 8. Note that the response surface presented in this figure represents in the z-axis the emissions predicted by the metamodel created for that case. The XY plane represents variables two (2) and three (3) of the 5-variable version of the problem. As explained above, they symbolize the eight variables associated with the dimensions of the columns (in the original 19-variable problem) grouped into two variables (Group Columns 1 and 2). To graph this response surface, the points belonging to the solution space of these two variables are plotted in order. At the same time, the other three take random values within their respective solution spaces. Therefore, this is a two-dimensional representation of the five-dimensional problem to exemplify how the proposed algorithm works graphically. These two variables have been selected because they have the same dimension (4096 values) and ensure that the XY plane is symmetric. The basic steps of the biphasic search algorithm are outlined below.

Step 1: Construction of the global metamodel using 100 points distributed by LHS and regression with a first-order polynomial (regpoli1). This choice is based on the experience of the previous study [37], combined with several trial-and-error tests. The figure shows an example of a cloud of points obtained in a DoE (red circles projected on the XY plane). Ten additional points also distributed by LHS are used to test the accuracy of the metamodel. The algorithm checks that these ten points do not coincide with the initial dataset. The actual values of these ten points are obtained through HFS. With these values, the mean absolute percentage error between the simulated and real response is calculated. If this average error is less than 5%, this step is completed, and the metamodel is considered good. If the error does not meet this criterion, the 10 points are added to the initial set, and another metamodel is built again, which is checked with another 10 points. This process is repeated until the criterion is met.

Step 2: Once the global metamodel is built, it is optimized by the base heuristic BBO. This process is repeated ten times (the computational consumption of optimization using LFS is negligible compared to the traditional one using HFS), and the best solution is chosen (KBO 1). This solution is updated with an HFS and checked for compliance with the constraints. If it does not, it is added to the initial cloud, and the metamodel is rebuilt and reoptimized until KBO 1 is feasible. For the case shown in Fig. 8, the solution KBO 1 = [140, 251, 798, 2455, 22] in the 5-variable version. This solution is transformed into its 19-variable version, and the CDLIS algorithm is applied to exploit the neighborhood using the actual model (HFS). The new solution achieved is called CDLIS 1. For the case represented, the values of the variables of CDLIS 1 are [1–6].

Step 3: The CDLIS 1 solution is transformed to its 5-variable version ([57, 157, 211, 3360, 1]), and a subspace is created by shrinking the limits to 15% of the initial size of each of the five variables. If the point is so close to a global boundary that half of 15% cannot be reached, the remainder is added in the other direction, as shown in Fig. 8. For the case explained, the new limits would be LB = [1, 1, 1, 1, 2868, 1] and UB = [454, 614, 614, 3852, 10]. In the figure, these limits are represented (for the two variables analyzed) with the thick red arrows.

Step 4: With these new boundaries, another metamodel is created, using 30 LHS points and the regression with a polynomial of order 0.

Step 5: This new local metamodel is optimized with BBO another ten times, and the best result is saved. This is called KBO 2, and for the process represented, the configuration of variable values is [57, 605, 258, 3838, 1]. The 5-variable solution is converted to its 19-variable version ([1–6]), and a local search is performed again. This solution is called CDLIS 2 and is considered the optimal one. For the reference case, CDLIS 2 = [1–6] for the final 19-variable version. In the 5-variable version, which is the one being represented in the figure, this final solution would be [57, 84, 17, 3290, 13]. The value of this final solution is 52282 kg CO_2, which has an accuracy of 99.42% compared to that obtained with a traditional heuristic procedure (51982 kg CO_2), saving 80% of computational consumption.

As can be seen, the CDLIS local search strategy is of great importance

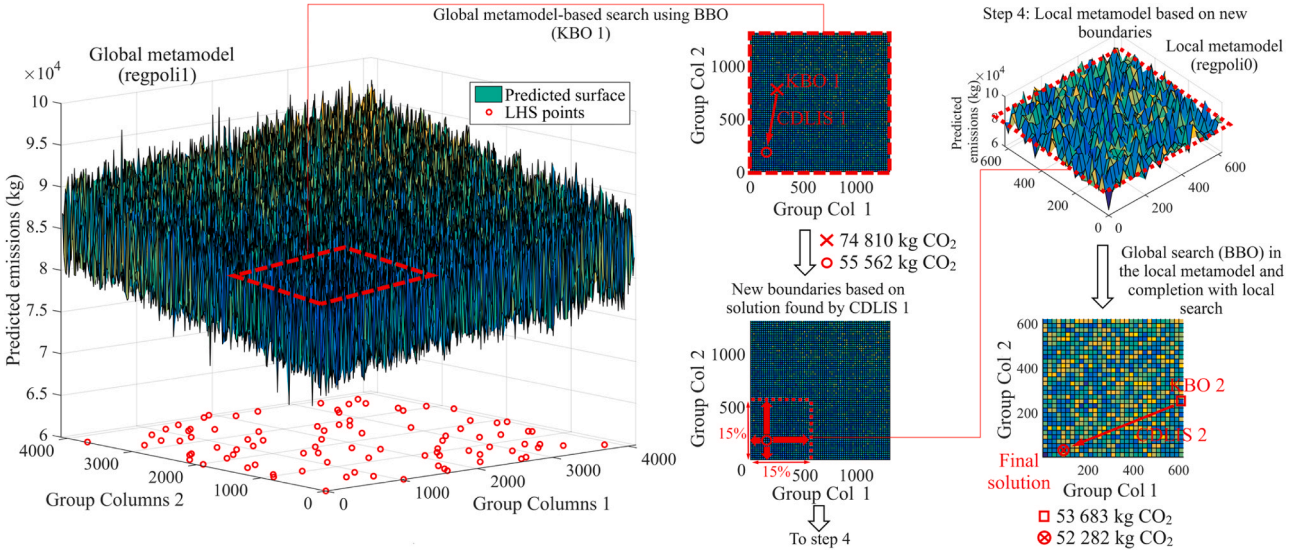

Fig. 8. Graphical illustration of the proposed metamodel-based metaheuristic. The solution represented belongs to the basic case study applying the ObRDPC framework for the failure of a corner column.

in the overall metaheuristic procedure. The improvement regarding the previously proposed version lies in gradually combining the individual solutions that improve the one that starts the iteration. In the original CDLIS, all the individual solutions that improve the basic are combined and tested as a single one. If it does not improve the basic, the best individual solution is established as the new basic solution, and the procedure is repeated. In this case, all the individual solutions that improved the basic one are combined randomly, starting with combining all of them. If the new solution obtained does not improve the basic, all but one of the solutions are randomly combined. If it continues without improvement, all but two are randomly combined, and so on, until no more solutions can be combined. If none improves the basic, the same is done as in the original, and the best individual is selected. For more information on this algorithm, refer to [37].

3. Results

The first section of the results focuses on checking the influence of slabs and infill walls on the structural robustness of the building in case of a load-bearing element failure. Then, the differences between the solutions optimized by traditional design and those obtained by applying the ObRDPC framework are compared. In this case, it is studied the influence of buildings' geometrical factors such as the number of levels and span length on their structural robustness. Finally, the differences observed in the structural elements as a function of the design approach are analyzed.

3.1. Impact of floor slabs and infill walls in RDPC

As mentioned, one of the essential points of this study is to examine how additional structural elements (slabs and walls) enhance the building's capacity to resist extreme events. Fig. 9 shows the optimal solutions obtained for each case study, where each structure is optimized without (grayscale bars) and with (colored bars) slabs/walls in the model. The first group of bars refers to the design using the classical approach. In contrast, the other two groups pertain to applying the ObRDPC framework while implementing the AP method and the corresponding design envelope. The first of these two groups corresponds to the loss of a corner column (APM CC), while the second represents cases where an exterior column is removed (APM EC). Therefore, this figure allows for analyzing the influence of slabs and walls on the optimal design for each case study, especially when RDPC is incorporated.

In the case of traditional design, the influence of these additional elements is not significant, especially when the span length is greater. The red line shows how the difference (in percent) between the models without and with slabs/walls tends to decrease. The results are the opposite for the cases where the ObRDPC framework is applied. Slabs and walls are more beneficial in models with longer span lengths. Eliminating a load-bearing element changes the structural behavior of the superstructure, and the presence of these additional elements is essential for stress redistribution (Fig. 10). The graphs show that, unlike traditional design, the additional structural elements lose effectiveness as the number of levels increases in the case of failure of a load-bearing component. This is because increasing the number of levels increases the number of structural components that "help" to redistribute and support the loads when the load-bearing element is eliminated.

In general, the additional structural elements represent a decrease of about 5.20% in emissions in the case of the traditional design. The beams are the most "grateful" for their presence, with an average reduction of 10.19%. Columns decrease by 1.69%, and foundations by 4.12%. In the case of a corner column loss, slabs and walls help reduce by an average of 11.07% the environmental cost of implementing RDPC (compared to a beam-column superstructure). Beams decrease by

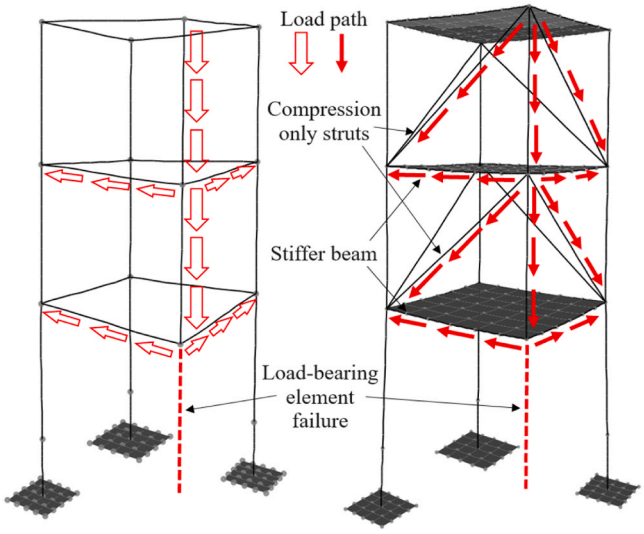

Fig. 10. Load redistribution after load-bearing element failure in frame structures without (left) and with (right) slab-walls.

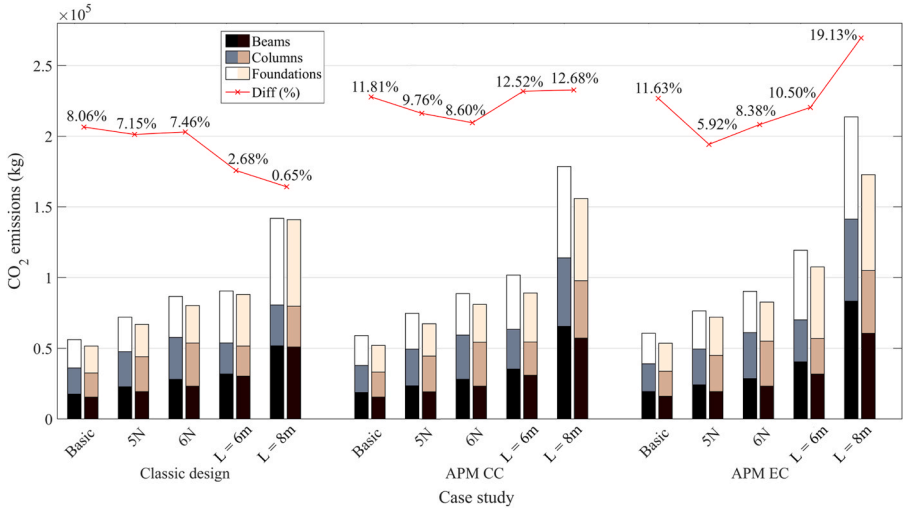

Fig. 9. Environmental cost of the optimized solutions for each case study using the beam-column models (grayscale bars) and those including additional structural elements (colored bars).

15.42%, columns by 8.68%, and foundations by 9.86%. For the loss of an exterior column, the additional elements result in environmental savings of 11.11% when implementing the ObRDPC framework. The environmental cost of beams is reduced by a significant 20.89% (especially for the $L = 8$ m model), columns reduce their cost by 9.83%, and foundations by 3.43%. Therefore, beams are the elements that benefit most from the presence of the additional structural components.

3.2. Comparison between traditional and RPC designs

Another significant aspect of this research is how constructing structurally robust buildings in abnormal situations impacts the environment. After confirming the impact of slabs and walls on structural robustness, all subsequent analyses are conducted using models that include these additional structural components. This evaluation of environmental cost focuses on two characteristics of the buildings: the number of levels and the span length.

3.2.1. Influence of number of levels and span length

One of the main characteristics that seems to influence the resistance of a building against collapse is the number of levels. It appears logical to think that the more levels the structure has, the weaker and more prone it should be to collapse. In addition, more levels mean more load to be redistributed/supported in case of failure of the load-bearing element.

However, Fig. 11 confirms the opposite. The increase in the number of levels seems to be a feature that increases the robustness of the structure. It is because, even when there is an increase in load to redistribute, the number of structural elements is also increased for this purpose. Note how the optimal designs based on the failure of a corner column are practically as costly as the traditional ones. The failure of an exterior column also does not seem to increase the environmental cost substantially. Note also that the beams do not change from one case to the other due to the presence of the slabs and walls, as discussed in the previous section. Columns and foundations are the elements responsible for absorbing load redistribution, although the differences are also negligible.

On the other hand, the span length does inversely affect the structural robustness of the building. Note in Fig. 12 that the differences are negligible up to the failure of a corner column for the $L = 6$ m model. After that, it becomes very costly to implement the PC-resistant design, especially if an exterior column fails. It is worth noting how this time, for the case of $L = 8$ m, the beams suffer significant cost variations, even with the structural assistance of slabs and walls. As in the previous instances (variation of N), the columns and foundations are the main ones responsible for resisting the redistribution of load.

3.2.2. Environmental cost of ObRDPC implementation as a function of V_I

It is necessary to unify the most significant characteristics of a building in a single term to visualize the differences described above. For this purpose, a metric called "volumetric index" is proposed, which includes parameters such as length/number of spans and height/number of levels. After finding that span length is directly and significantly proportional to the higher environmental cost of structures resistant to PC, it directly affects the index. Other terms, such as the number of levels and spans, affect it indirectly. Eq. 15 expresses this index, an abstract concept applicable to structures with symmetrical spans and levels.

$$V_I = (L_L * L_B * N_i) * \left(\frac{1}{N} + \frac{1}{N_L} + \frac{1}{N_B}\right) \tag{15}$$

Here, L_L, L_B, and N_i are the lengths of the spans on the x-axis, y-axis, and the height of each level, respectively. This first term represents the volume of each sub-cube of the overall 3D frame. N, N_L, and N_B are the number of levels, spans in the x-axis direction, and spans in the y-axis direction, respectively.

Fig. 13 shows the relationship of V_I with the environmental cost increase when applying ObRDPC compared to the traditional design. Note that curves symbolizing the five case studies are plotted for the two implemented column failures. In addition, the differences in models with (red curves) and without (black curves) the additional structural elements are plotted. Since the points follow this pattern, these curves are obtained by a logarithmic fit (except APM CC WITH slabs and walls). The most important conclusion demonstrated by this graph is the very positive influence of slabs and walls on the structural robustness of the buildings. The most significant impact of these additional elements occurs in buildings with higher indexes, basically in those with longer spans. In these buildings, it is extremely costly to implement a robust-to-collapse design, exceeding a 50% increment for the case of $L = 8$ m. However, by constructing the slabs and walls in a way that affects the overall behavior of the superstructure, it is possible to design robust buildings to PC while increasing the environmental impact by less than 25%. Even so, these increases are quite significant, suggesting that it is necessary to look for other alternatives for buildings with spans greater than 6 m.

As discussed in Section 3.1, the main reason for this behavior is the redistribution of forces caused by the presence of slabs and walls in response to the loss of the load-bearing element (see Fig. 10). This more

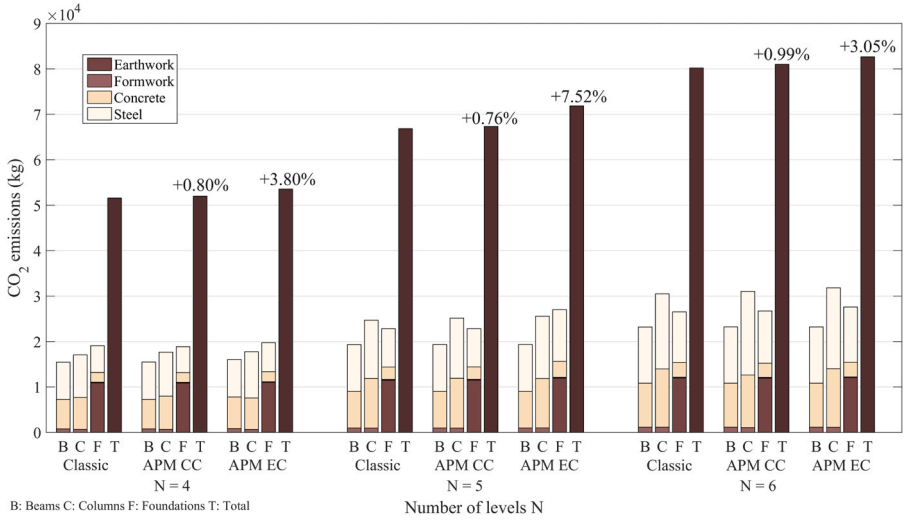

Fig. 11. Comparison in environmental terms of the optimal design results (broken down into elements and their corresponding components/activities) as a function of the number of levels N.

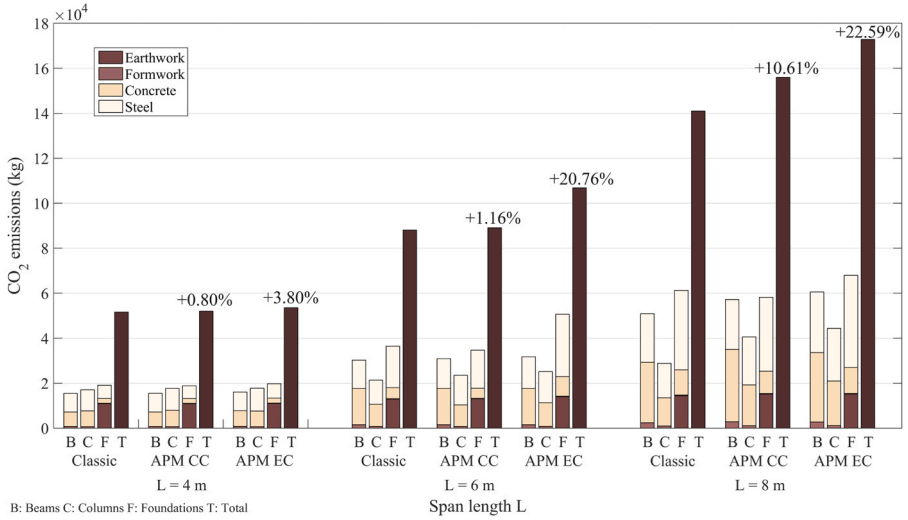

Fig. 12. Comparison in environmental terms of the optimal design results (broken down into elements and their corresponding components/activities) as a function of the span length *L*.

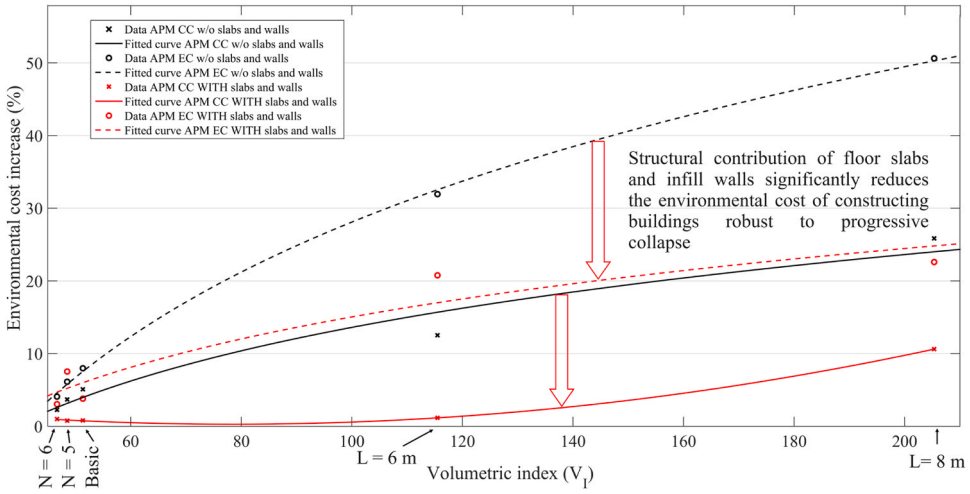

Fig. 13. Behavior of the environmental cost increase (when implementing ObRDPC) as a function of the volumetric index. APM: Alternate Path Method. CC: corner column. EC: exterior column.

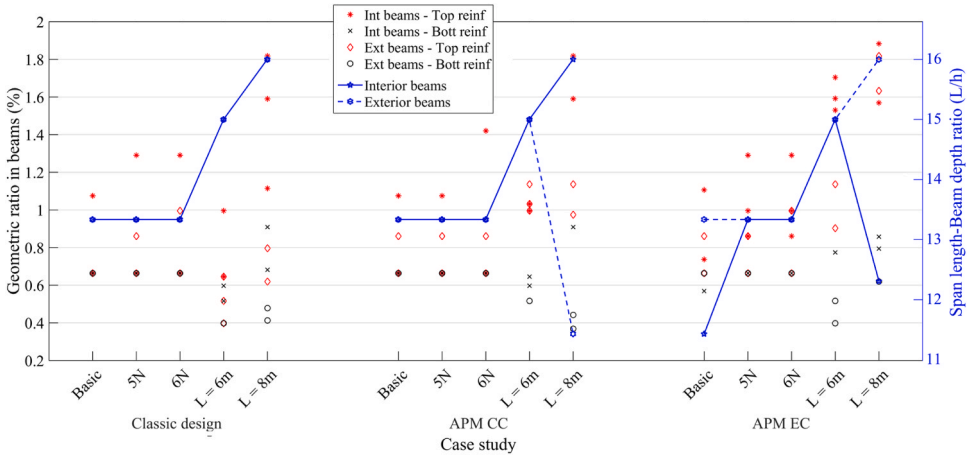

Fig. 14. Geometric and *L/h* ratios in beams for each case study as a function of the optimization-based design method.

efficient redistribution is particularly beneficial for the beams, which can more effectively handle the increasing demands resulting from the column failure. This phenomenon, where alternative load paths are activated more efficiently due to the presence of additional elements, becomes more significant as the span of the beams increases.

3.3. Structural behavior of each element type

This section further analyzes the structural behavior of beams, columns, and foundations to resist the loss of the load-bearing element. Consequently, the differences between traditionally designed (and optimized) elements and when applying the ObRDPC framework are presented. The case studies analyzed are those that include slabs and walls in the model.

3.3.1. Beams

Fig. 14 shows the behavior of two properties, the span-to-depth ratio and the geometric ratio (ratio of steel to concrete area) of each group of beams for each case study. The first property (L/h, blue lines) shows that the beams do not undergo many changes between the traditional and the progressive-collapse-resistant design, as stated in previous sections. The only cases that have increased their depth compared to the traditional design are (a) the exterior beams in the $L = 8$ m model for the loss of the corner column, (b) the interior beams of the basic case for the loss of the exterior column, and (c) the interior beams in the same failure situation for the $L = 8$ m model.

The other property referring to the amount of steel as a function of concrete does not reveal significant changes either, except for the failure of the exterior column. Note the increase of the top reinforcement (red symbols), especially for the cases of $L = 6$ and 8 m. Generally, neither the beams' top nor bottom reinforcement increases significantly for corner column failure. For the case of exterior column failure, the bottom reinforcement does not increase significantly either, while the top reinforcement increases by 37% compared to the traditional design. In this case, the exterior beams stand out with an increase of 47%, mainly in the models with larger spans. To get an idea of the influence of the additional structural elements, in the models with beam-column typology (without slabs/walls), the upper reinforcement in interior beams increases by 32% due to the loss of an exterior column. The exterior beams increase their steel geometric ratio by 60% in both failure cases.

3.3.2. Columns

The columns are elements that significantly change from the traditional design to the progressive-collapse-resistant one. It is not only the increase in cost but also the cross-section rectangularity of their groups. For this type of structure, it is essential to highlight the predominance of bending due to gravity loads. The columns that do not have this predominance (e.g., interior and corner in the traditional design approach) tend to seek their optimal shape to improve the stiffness of the building against horizontal loads (wind, in this case). On the other hand, the exterior columns in both directions seek their shape to deal with the predominance of bending due to gravity loads. Note how, in the classic design, the x-axis exterior columns (Ext-X, "x" in Fig. 15) have optimum rectangularities of less than 1 (are located below the red line). The exterior columns in the y-axis (Ext-Y, diamonds in Fig. 15) change their rectangularity, and their largest side is in the x-axis direction (above the red line). Notice how the other groups distribute their sections so that there is no predominance of rectangularity in any direction. The points do not tend to be distributed in the same area (do not saturate the graph on either side of the red line) but are symmetrically distributed. Even if the points on one side of the red line move away from it, the same thing happens on the other side. This symmetry means that the stiffness in both directions is well distributed.

Note that the rectangularities tend to decrease during corner column failure. The most critical aspect in both failure cases is that the exterior columns change their optimal configuration. Now, the x's are above the red line (largest side on the x-axis), and the diamonds tend to be below (largest side on the y-axis). Another aspect that stands out is that for the failure of the corner column, the remaining columns of this group tend to be square (or with low rectangularity). On the contrary, for the failure of the exterior column, its optimum shape tends to be with the largest side in the x-axis direction to deal with the increase in bending that produces the loss of the load-bearing element. The opposite is true for interior columns. I.e., little or no rectangularity at the corner column failure, and shapes that tend to have the larger side in the y-axis direction while the exterior column fails.

Overall, the average rectangularity in the classic design is 1.09 for interior columns, 0.69 for Ext-X columns, 1.44 for Ext-Y columns, and 1.12 for corner columns. The total average rectangularity is 1.08, reaffirming the symmetry mentioned above. For the APM CC design, the average rectangularities are 1.03, 1.17, 0.90, and 1.00, respectively, with an overall average of 1.03. For the exterior column failure (APM EC), the distribution would be 0.77, 1.15, 0.96, and 1.34, for an average of 1.05.

This means that each type of design has its particularities, and even if specific common patterns are met, certain groups tend to change radically from one design approach to another. Therefore, the best solution would be to establish all situations and create an optimized envelope to achieve the best overall layout that is efficient in all scenarios.

3.3.3. Foundations

Fig. 16 clarifies the tendency to use square footing in the case of

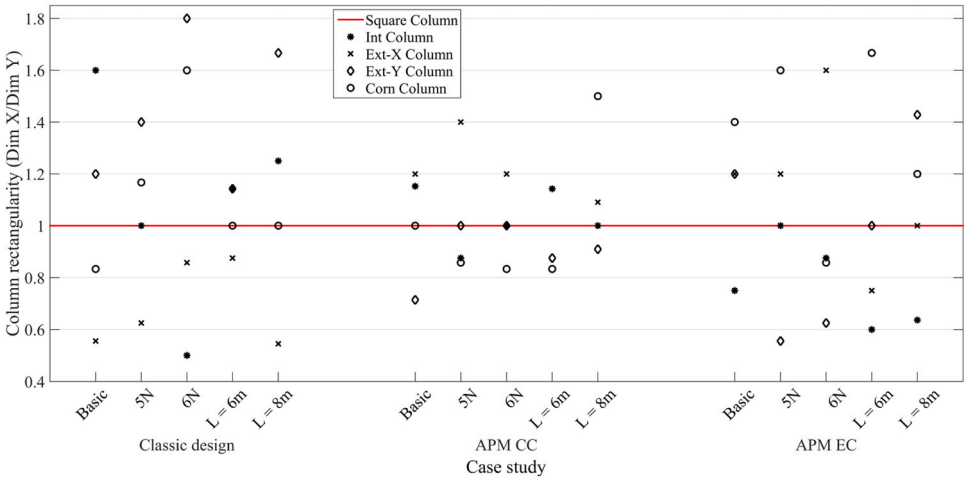

Fig. 15. Rectangularity of column groups as a function of the optimization-based design method.

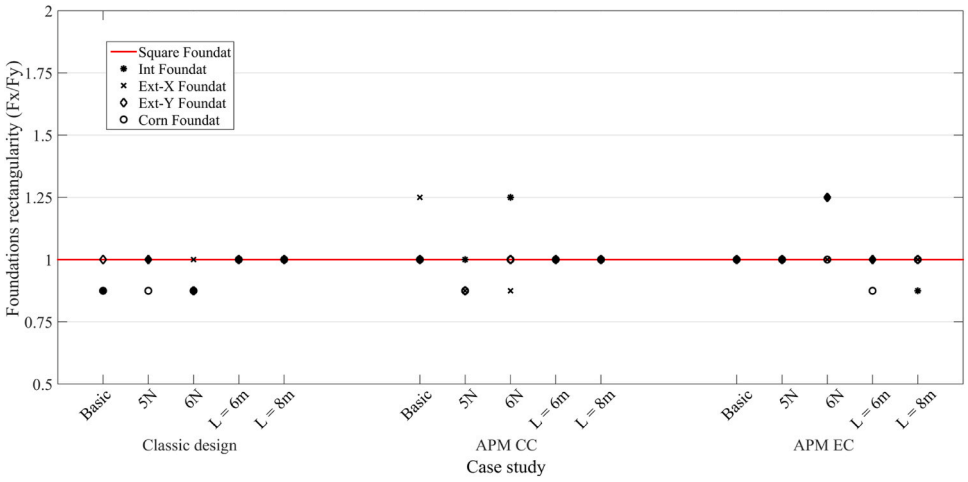

Fig. 16. Rectangularity of foundation groups as a function of the optimization-based design method.

foundations. What changes from one design approach to the other is the area of the foundation footing, which is directly related to the increase in environmental cost at the failure of the load-bearing element compared to the classical design. Recall that the dynamic amplification coefficient is not used for load combinations to design the foundations in the failure state. Therefore, this increase is only due to resisting the extra load resulting from the eliminated load-bearing element.

The interior foundations do not increase their area when the corner column fails. However, failure of the exterior column causes a 20% increase in the base area of this group of elements. Both groups of exterior foundations increase their footing area by 8% in both failure cases. The corner foundations do not suffer significant changes in the failure of the corner column, but they do increase their base by a considerable 36% when the exterior column fails.

3.4. *Future lines of research*

With the application of the ObRDPC framework, it has been possible to design buildings resilient to extreme events while minimizing the environmental impact of their construction. Aspects often overlooked, such as the influence of slabs and walls on structural robustness or the soil-structure interaction, have been considered within the methodology developed. However, this field needs further exploration, and much research remains.

One of the areas for development within the framework is improving the design envelope. Its current version evaluates the failure of corner and exterior columns independently. Future studies should combine all possible failures (including interior positions) to create a more comprehensive envelope. This will make each function evaluation even more computationally expensive.

Considering a more comprehensive design envelope will make the building structurally more robust. However, this entails higher material consumption and a greater negative environmental impact. An alternative to further enhance the influence of additional structural elements, such as slabs, is to include them in the design optimization process. Optimizing slab design as part of the structural assembly would allow for regulating its influence on collapse resistance, potentially leveraging phenomena overlooked in this study, such as the tensile membrane action.

A critical area for improvement is updating the methodology used to evaluate and design buildings for robustness against collapse. This research employed the AP method according to the GSA code guidelines. Nonetheless, recent practical studies indicate that these codes require revisions. Consequently, the developed tool must also be updated to enhance structural robustness. Another potential improvement involves integrating multiple codes to address procedural shortcomings. For example, the guidelines used in this study do not explicitly account for the effects of catenary action when an exterior or interior load-bearing element fails. In contrast, other approaches, such as the Tie Forces method found in another codes, do consider this effect. Combining methodologies could, therefore, refine and strengthen the procedure.

Another point to be explored is the implementation of seismic-resistant design. Instead of a static approach, performing dynamic analysis is another alternative applicable to the basic methodology proposed in this study. It involves making changes such as using the Nonlinear Dynamic Procedure for the AP method or considering another type of element (instead of Winkler-type) to simulate the SSI, such as Kelvin- or Maxwell-type elements.

All of the above makes the problem formulated, which is already difficult to solve, even more complex. Therefore, an important area for further exploration is the role of metamodels in enhancing the convergence of optimization processes. This study uses the metamodel to guide the global search in a two-phase approach, while a local optimization algorithm refines the search using HFS. This strategy ensures computational efficiency while minimizing the demand for exceptional metamodel accuracy, as achieving such precision would impose significant computational costs. This trade-off highlights an opportunity to investigate alternative strategies for constructing the DoE or adopting different types of metamodel techniques. Such methods could improve the efficiency of the global search phase while reducing the dependence on local refinement via HFS. Although the proposed algorithm already achieves substantial computational savings, future work could focus on strategies that further improve this balance, potentially yielding even greater efficiency.

4. Concluding remarks

Even though several studies on building design optimization have been developed, implementing safety criteria is a subject that needs to be deepened. One of the points associated with structural safety that has been gaining significant interest from the scientific community is the PC resistance of structures, especially buildings. Many numerical and experimental studies have been implemented to investigate the basic principles of this phenomenon. However, only some authors have combined it with structural optimization to design safer and more resilient, yet sustainable buildings.

This research relates these two issues by proposing and applying a methodology called the ObRDPC framework. It combines two design approaches: the traditional one based on the Limit States and the one considering the PC resistance according to the Alternate Path method proposed by codes such as the GSA. Meanwhile, an optimization algorithm supervises minimizing the CO_2 emissions required to construct the

building. This methodology also suggests a strategy to consider a usually ignored aspect, such as SSI. In addition, alternative structural elements such as slabs and walls are modeled as part of the superstructure frame, another aspect usually ignored in studies of this nature.

Due to the complex optimization problem formulated, it is necessary to design a metaheuristic based on a biphasic search aided by Kriging-type metamodels. A local search algorithm developed for this type of problem is also implemented within the global metaheuristic. The method reduced the computational consumption by about 80% while maintaining the accuracy of the results at more than 99%. The results yield several interesting conclusions:

- Slabs and structural walls are essential for improving the PC resistance of buildings, especially those with considerable span length. Their presence helps reduce an average of 11% of the total emissions required to build resilient structures. Beams are the structural elements that are most "grateful" for their presence in dealing with the loss of load-bearing elements.
- Increasing the number of levels of a building increases its capacity to be resilient to the loss of a load-bearing element, especially if the contribution of slabs and walls is not considered. In other words, implementing a PC-robust design in a building with more levels is generally less polluting than in buildings with fewer levels. On the other hand, increasing the span length does make implementing RDPC extremely environmentally costly from an environmental point of view. However, the presence of slabs and structural walls helps to reduce this negative impact.
- In buildings where slabs and walls are structurally modeled, the beams stay mostly the same from the traditional approach to the robust to PC design. The most significant differences are seen in the top reinforcing steel in buildings with spans greater than 6 m and for the loss of an exterior column. The cross-section's rectangularity of the exterior columns varies significantly between traditional and structurally robust designs. The foundation undergoes some changes for each design approach, especially the footing area, not its rectangularity.

CRediT authorship contribution statement

Moacir Kripka: Writing – review & editing, Validation, Supervision, Methodology, Funding acquisition, Conceptualization. **Víctor Yepes:** Writing – review & editing, Validation, Supervision, Resources, Project administration, Methodology, Investigation, Funding acquisition, Conceptualization. **Iván Negrin:** Writing – original draft, Visualization, Validation, Software, Methodology, Investigation, Formal analysis, Data curation, Conceptualization.

Declaration of Competing Interest

The authors declare that they have no known competing financial interests or personal relationships that could have appeared to influence the work reported in this paper.

Acknowledgments

This work was supported by the Grant PID2023-150003OB-I00 funded by MICIU/AEI/10.13039/501100011033 and by "ERDF/EU". Grant PRE2021–097197 funded by MICIU/AEI/10.13039/501100011033 and by FSE+ . Grant CNPq 305484/2023-0 funded by the Brazilian National Council for Scientific and Technological Development.

Data Availability

Data will be made available on request.

References

[1] Sánchez-Garrido AJ, Navarro IJ, Yepes V. Multi-criteria decision-making applied to the sustainability of building structures based on modern methods of construction. J Clean Prod 2022;330:129724. https://doi.org/10.1016/j.jclepro.2021.129724.
[2] Navarro IJ, Yepes V, Martí JV. A review of multicriteria assessment techniques applied to sustainable infrastructure design. Adv Civ Eng 2019:6134803. https://doi.org/10.1155/2019/6134803.
[3] Kim SH, Kwak HG. Optimization of an RC frame structure based on a plastic analysis and direct search of a section database. J Build Eng 2022;48. https://doi.org/10.1016/j.jobe.2021.103959.
[4] Kaveh A, Rezazadeh Ardebili S. Optimum design of 3D reinforced concrete frames using IPGO algorithm. Structures 2023;48. https://doi.org/10.1016/j.istruc.2023.01.071.
[5] Mergos PE. Sustainable and resilient seismic design of reinforced concrete frames with rocking isolation on spread footings. Eng Struct 2023;292. https://doi.org/10.1016/j.engstruct.2023.116605.
[6] Xiang Y, Mahamadu AM, Florez-Perez L, Wu Y. Design optimisation towards lower embodied carbon of prefabricated buildings: balancing standardisation and customisation. Dev Built Env 2024;18. https://doi.org/10.1016/j.dibe.2024.100413.
[7] Negrin I, Chagoyén E. Economic and environmental design optimisation of reinforced concrete frame buildings: a comparative study. Structures 2022;38:64–75. https://doi.org/10.1016/j.istruc.2022.01.090.
[8] Lao WL, Li M, Wong BCL, Gan VJL, Cheng JCP. BIM-based constructability-aware precast building optimization using optimality criteria and combined non-dominated sorting genetic II and great deluge algorithm (NSGA-II-GD). Autom Const 2023;155. https://doi.org/10.1016/j.autcon.2023.105065.
[9] Tanhadoust A, Madhkhan M, Nehdi ML. Two-stage multi-objective optimization of reinforced concrete buildings based on non-dominated sorting genetic algorithm (NSGA-III). J Build Eng 2023;75. https://doi.org/10.1016/j.jobe.2023.107022.
[10] Negrin I, Kripka M, Yepes V. Multi-criteria optimization for sustainability-based design of reinforced concrete frame buildings. J Clean Prod 2023;425. https://doi.org/10.1016/j.jclepro.2023.139115.
[11] Yuan Z, Man Q, Guan Z, Yi C, Zheng M, Chang Y, Li HX. Simulation and optimization of prefabricated building construction considering multiple objectives and uncertain factors. J Build Eng 2024;86. https://doi.org/10.1016/j.jobe.2024.108830.
[12] Adam JM, Parisi F, Sagaseta J, Lu X. Research and practice on progressive collapse and robustness of building structures in the 21st century. Eng Struct 2018;173:122–49. https://doi.org/10.1016/j.engstruct.2018.06.082.
[13] Caredda G, Makoond N, Buitrago M, Sagaseta J, Chryssanthopoulos M, Adam JM. Learning from the progressive collapse of buildings. Dev Built Env 2023;15. https://doi.org/10.1016/j.dibe.2023.100194.
[14] General Services Administration (GSA). Alternate Path Analysis And Design Guidelines For Progressive Collapse Resistance. Washington, DC: Office of Chief Architects,; 2013.
[15] Department of Defense (DoD), Design of buildings to resist progressive collapse (UFC 4–023-03), Washington, DC: Unified Facilities Criteria, 2009.
[16] Fascetti A, Kunnath SK, Nisticò N. Robustness evaluation of RC frame buildings to progressive collapse. Eng Struct 2015;86:242–9. https://doi.org/10.1016/j.engstruct.2015.01.008.
[17] Feng FF, Hwang HJ, Zhou Y, Sun JM, Zhang HZ, Roh JH, Kang SM, Yi WJ. Effect of three-dimensional space on progressive collapse resistance of reinforced concrete frames under various column removal scenarios. J Build Eng 2024;90. https://doi.org/10.1016/j.jobe.2024.109405.
[18] Kai Qian, Li Bing. Dynamic performance of RC beam-column substructures under the scenario of the loss of a corner column—experimental results. Eng Struct 2012;42:154–67. https://doi.org/10.1016/j.engstruct.2012.04.016.
[19] Ma F, Gilbert BP, Guan H, Xue H, Lu X, Li Y. Experimental study on the progressive collapse behaviour of RC flat plate substructures subjected to corner column removal scenarios. Eng Struct 2019;180:728–41. https://doi.org/10.1016/j.engstruct.2018.11.043.
[20] Kim SH, Lee BM, Kang SM, Hwang HJ, Choi H, Ma G. Simplified test method for evaluating progressive collapse resistance of precast concrete frame structures. J Build Eng 2024;88. https://doi.org/10.1016/j.jobe.2024.109236.
[21] Y. Bao, J.A. Main, S.Y. Noh, Evaluation of Structural Robustness against Column Loss: Methodology and Application to RC Frame Buildings, J. Struct. Eng. 142(8), https://doi.org/10.1061/(ASCE)ST.1943–541X.0001795.
[22] H. Helmy, H. Salem, S. Mourad, Computer-Aided Assessment of Progressive Collapse of Reinforced Concrete Structures according to GSA Code, J. Perform. Constr. Facil. 27(5), https://doi.org/10.1061/(ASCE)CF.1943–5509.0000350.
[23] Parisi F, Scalvenzi M. Progressive collapse assessment of gravity-load designed European RC buildings under multi-column loss scenarios. Eng Struct 2020;209. https://doi.org/10.1016/j.engstruct.2019.110001.
[24] Shan L, Petrone F, Kunnath S. Robustness of RC buildings to progressive collapse: Influence of building height. Eng Struct 2019;183:690–701. https://doi.org/10.1016/j.engstruct.2019.01.052.
[25] Lim NS, Tan KH, Lee CK. Experimental studies of 3D RC substructures under exterior and corner column removal scenarios. Eng Struct 2017;150:409–27. https://doi.org/10.1016/j.engstruct.2017.07.041.
[26] M. Guo, H. Huang, W. Zhang, C. Xue, M. Huang, Assessment of RC Frame Capacity Subjected to a Loss of Corner Column, J. Struct. Eng. 148(9), https://doi.org/10.1061/(ASCE)ST.1943–541X.0003423.

[27] Makoond N, Setiawan A, Buitrago M, Adam JM. Arresting failure propagation in buildings through collapse isolation. Nature 2024;629:592–6. https://doi.org/10.1038/s41586-024-07268-5.
[28] Li S, Wang H, Liu H, Shan S, Zhai C. Experimental study on progressive collapse of self-centering precast concrete frame with infill walls. Eng Struct 2023;294. https://doi.org/10.1016/j.engstruct.2023.116746.
[29] Nyunn S, Wang F, Yang J, Liu QF, Azim I, Bhatta S. Numerical studies on the progressive collapse resistance of multi-story RC buildings with and without exterior masonry walls. Structures 2020;28:1050–9. https://doi.org/10.1016/j.istruc.2020.07.049.
[30] Buitrago M, Bertolesi E, Sagaseta J, Calderón PA, Adam JM. Robustness of RC building structures with infill masonry walls: tests on a purpose-built structure. Eng Struct 2021;226. https://doi.org/10.1016/j.engstruct.2020.111384.
[31] Beck AT. Optimal design of redundant structural systems: fundamentals. Eng Struct 2020;219. https://doi.org/10.1016/j.engstruct.2020.110542.
[32] Beck AT, da Rosa Ribeiro L, Valdebenito M. Risk-based cost-benefit analysis of frame structures considering progressive collapse under column removal scenarios. Eng Struct 2020;225. https://doi.org/10.1016/j.engstruct.2020.111295.
[33] Beck AT, Stewart MG. Risk-based cost-benefit analysis of structural strengthening to mitigate disproportionate collapse of buildings under abnormal blast loading. Structures 2023;57. https://doi.org/10.1016/j.istruc.2023.105103.
[34] da Rosa Ribeiro L, Machado Kroetz H, Parisi F, Beck AT. Optimal risk-based design of reinforced concrete beams against progressive collapse. Eng Struct 2024;300. https://doi.org/10.1016/j.engstruct.2023.117158.
[35] Beck AT, da Rosa Ribeiro L, Costa LGL, Stewart MG. Comparison of risk-based robustness indices in progressive collapse analysis of building structures. Structures 2023;57. https://doi.org/10.1016/j.istruc.2023.105295.
[36] Esfandiari MJ, Urgessa GS. Progressive collapse design of reinforced concrete frames using structural optimization and machine learning. Structures 2020;28. https://doi.org/10.1016/j.istruc.2020.09.039.
[37] Negrin I, Kripka M, Yepes V. Metamodel-assisted meta-heuristic design optimization of reinforced concrete frame structures considering soil-structure interaction. Eng Struct 2023;293. https://doi.org/10.1016/j.engstruct.2023.116657.
[38] K. Ozgan, S. Kılıçer, A.T. Daloglu, Soil–Structure Interaction Effect on the Resistance of a Steel Frame against Progressive Collapse Using Linear Static and Nonlinear Dynamic Procedures, J. Perform. Constr. Facil. 37(1), https://doi.org/10.1061/JPCFEV.CFENG-4181.
[39] Ozgan K, Kılıçer S, Daloglu AT. Evaluation of progressive collapse potential of a RC school building considering soil–structure interaction. Asian J Civ Eng 2023;24:1199–213. https://doi.org/10.1007/s42107-022-00562-5.
[40] Negrin I, Roose D, Chagoyén E, Lombaert G. Biogeography-Based Optimization of RC structures including static soil structure interaction. Struct Eng Mech 2021;80(3):285–300. https://doi.org/10.12989/sem.2021.80.3.285.
[41] Mohamed OA. Assessment of progressive collapse potential in corner floor panels of reinforced concrete buildings. Eng Struct 2009;31:749–57. https://doi.org/10.1016/j.engstruct.2008.11.020.
[42] Garg S, Agrawal V, Nagar R. Case study on strengthening methods for progressive collapse resistance of RC flat slab buildings. Structures 2021;29:1709–22. https://doi.org/10.1016/j.istruc.2020.12.049.
[43] Naser MZ. Autonomous and resilient infrastructure with cognitive and self-deployable load-bearing structural components. Autom Constr 2019;99:59–67. https://doi.org/10.1016/j.autcon.2018.11.032.
[44] Makoond N, Shahnazi G, Buitrago M, Adam JM. Corner-column failure scenarios in building structures: Current knowledge and future prospects. Structures 2023;49. https://doi.org/10.1016/j.istruc.2023.01.121.
[45] ASCE/SEI. Standard 41-06: Seismic Rehabilitation Of Existing Structures, 2007. Reston, Virginia, USA: ASCE,; 2007.
[46] Catalonia Institute of Construction Technology. BEDEC PR/PCT ITEC material database; 2016.
[47] Klepikov SN. General Solution For Beams And Plates On Elastically Deforming Bases With Varying Stiffnesses. In: Bases, foundations and soil mechanics research. Kiev: Budivielnik,; 1969. p. 37–47.
[48] Negrin I, Kripka M, Yepes V. Metamodel assisted design optimization in the field of structural engineering: a literature review. Structures 2023;52:609–31. https://doi.org/10.1016/j.istruc.2023.04.006.
[49] Simon D. Biogeography-based optimization. IEEE Trans Evolut Comput 2018;12(6):702–13. https://doi.org/10.1109/TEVC.2008.919004.
[50] Negrin I, Kripka M, Yepes V. Design optimization of welded steel plate girders configured as a hybrid structure. J Constr Steel Res 2023;211. https://doi.org/10.1016/j.jcsr.2023.108131.